Development of MRI Brain Image Segmentation-technique with Pixel Connectivity

S. Abdalla[*] and N. Al-Aama[**] Maryam A. Al-Ghamdi[***]

[*]Department, Institute Name [1]Department of Medical Physics, Faculty of Science, King Abdulaziz University Jeddah, P.O. Box 80203, Jeddah 21589, Saudi Arabia, smabdullah@kau.edu.sa, Tel. 00966 5823438322
[**]Internal Medicine and Cardiology, King Abdulaziz University Medical School, Present Director of CCU & Consultant Adult Interventional Cardiologist, dr_nabilalama@yahoo.com
[***]Department of Biochemistry, Faculty of Science, King Abdulaziz University Jeddah, P.O. Box 80203, Jeddah 21589, Saudi Arabia
maaalghamdi3@kau.edu.sa

***Abstract*-**Recently, Magnetic Resonance Imaging (MRI) of Brain is used widely in the clinical applications for the detection of abnormalities such as tumor. Accurate segmentation of the affected regions in the brain MRI image plays a vital role in the quantitative image analysis to detect the location of tumor in the brain. However, many segmentation algorithms suffer from limited accuracy, due to the presence of noise and intensity inhomogeneity in the brain MR images. This paper proposes a novel Textural Pixel Connectivity (TPC) based segmentation technique to predict the location of brain tumor. The Probabilistic Neural Network (PNN) classifier is used to classify the normal and abnormal images. If the image is classified as abnormal, then TPC segmentation process is applied for clustering out the background and tumor spot in the binary segmented output. Then, the growing pattern of tumor is analyzed and represented as a binary image output. The proposed technique achieves superior performance in terms of sensitivity, specificity, accuracy, error rate, correct rate, inconclusive rate, Positive Predicted Values (PPV), Negative Predicted Values (NPV), classified rate, prevalence, positive likelihood and negative likelihood, when compared to the traditional Adaboost and Enhanced Adaboost techniques.

***Index Terms*-** Affine Transform, Brain Tumor detection, Canny-based Edge Detection, Fractional Fourier Transform (FRFT), Gaussian Mixture Model (GMM), Enhanced Gray Level Co-occurrence Matrix (GLCM), Magnetic Resonance Imaging (MRI) Brain Image, Probabilistic Neural Network (PNN) classifier, Textural Pixel Connectivity (TPC) based segmentation.

I. INTRODUCTION

Image segmentation [1], [2] has gained more popularity and attracted more attention in medical field. This helps in the effective and early diagnosis and detection of brain tumor. For the early detection of brain tumors, various imaging techniques such as Positron Emission Tomography (PET), Magnetic Resonance Imaging (MRI), and Computed Tomography (CT) are used. Among them, Magnetic Resonance Imaging (MRI) is high-quality medical imaging technique that enables reliable and rapid detection of brain tumor. This is due to less harmful radiation, high contrast of soft tissues and high spatial resolution. MRI provides rich information about the anatomical structure to enable quantitative clinical examination. Highly accurate segmentation is required for the quantification of tumor in the MRI brain image. The size, shape and location of the brain tumors can vary for each individual. In addition to the tumor heterogeneity, the edges of the tumor may be complex and visually vague to detect. Some tumors may deform the surrounding structures in the brain. Additionally, presence of artifacts and noise in the brain tumor images increase the difficulty in tumor detection. Thus, designing an efficient and automatic image segmentation approach is necessary to provide a better tumor detection performance. Figure 1 shows the brain MRI images containing tumor and non-tumor brain image.

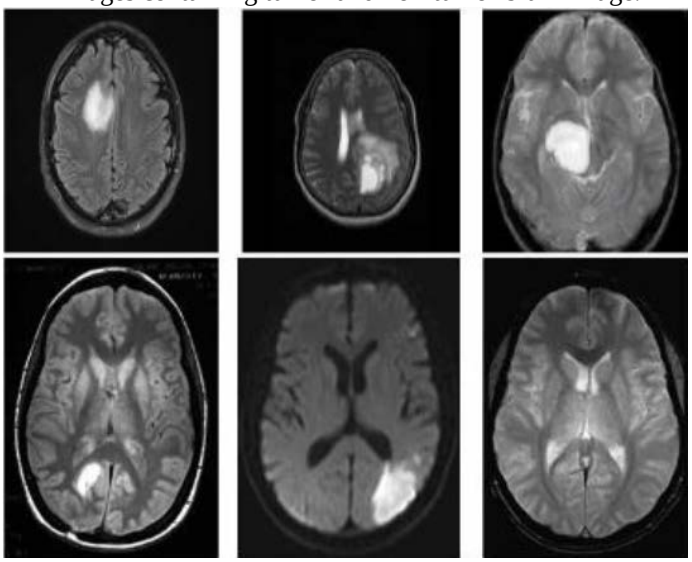

Figure 1 Brain MRI images containing tumor and Non-tumor brain image

Numerous approaches have been proposed during the last two decades for brain image segmentation. Existing image segmentation approaches are thresholding [3], region-based [4] and edge-based segmentation [4]. However, these approaches do not produce adequate and accurate segmentation results, due to the presence of noise and inhomogeneous intensities in the image. Occurrence of inhomogeneous intensities in the brain MRI images may cause due to the bias field and heavy noise. The presence of noise and artifacts in the brain images increases the difficulty in the segmentation of tumor. Due to the variation in the size, shape, location and heterogeneity of the brain tumors, detection of the edges of the tumors is highly complex and visually vague. Some tumors cause deformation of the surrounding structures in the brain, due to the mass effect or edema. Heterogeneity of tissue causes the potential rise in the

uncertainty of the segmentation task. Moreover, the presences of redundant and noisy features increase the computational complexity and degrade the performance of segmentation process. Accordingly, selection of relevant and informative features from redundant measurements is really crucial to improve the segmentation accuracy. Hence, this paper proposes a novel TPC based brain MRI image segmentation technique for the effective detection of location of brain tumor. Adaptive median filtering is performed as a pre-processing technique to remove the noise such as impulse noise from the brain MRI image. Canny-based Edge Detection is used for detecting edge of skull from MRI brain image. Extraction of the pixel components is performed to verify the presence of unwanted pixels. The Morphological operation is applied to eliminate the skull from the input MRI image. Then, the Gaussian Mixture Model (GMM)-based intensity equalization method enhances the contrast of the image. Feature extraction is done by using the enhanced Gray level Co-occurrence Matrix (GLCM) method. The PNN classifier performs classification of normal and abnormal images. The affine transform combined with Fractional Fourier Transform (FRFT) is applied to extract the texture of tumor intensity level from the given input image. If the input image is classified as an abnormal image, then segmentation is done by using TPC segmentation process. Then, the growing pattern of tumor is analyzed and represented as a binary image output. By performing the segmentation after the classification of the abnormal image, the proposed technique enables efficient reduction in the overall time required for the brain MRI image analysis. Finally, the performance of the PNN classifier is evaluated by comparing it with traditional Adaboost and enhanced Adaboost. The proposed technique achieves superior performance in terms of sensitivity, specificity, accuracy, error rate, correct rate, inconclusive rate, PPV, NPV, classified rate, prevalence, positive likelihood and negative likelihood. The remaining of the paper is systematized as follows: Section II describes the existing MRI brain image segmentation techniques. Section III explains about the proposed TPC segmentation technique including adaptive median filter, enhanced GLCM based feature extraction process, PNN classification method and segmentation process. The performance evaluation results of the proposed technique are illustrated in the section IV. Section V discusses about the conclusion and future implementation of the proposed work.

II. MRI BRAIN IMAGE SEGMENTATION TECHNIQUES

This section explains about the conventional image segmentation approaches applied for the segmentation of MRI brain images. Automatic segmentation of brain tissues from the MRI image plays an important role in the healthcare application and research fields. Robust segmentation of brain tissues is enabled by identifying the characteristic information among the multiple features extracted on the super pixels. There are some difficulties in the clustering process due to the heterogeneity of tissues and redundancy of the MRI features. To overcome these challenges, Kong et al [5] introduced a robust discriminative segmentation method based on the information theoretic learning approach. The informative feature was selected simultaneously and uncertainties of super voxel assignment were reduced. Hence, effective discriminative segmentation of the brain tissue was achieved. Ji et al [6] proposed a novel Adaptive Scale Fuzzy Local Gaussian Mixture Model (AS-FLGMM) algorithm for the accurate and robust segmentation of the brain MR image. The proposed approach was implemented in both real-time and simulated clinical MR images and compared with the existing segmentation approaches. The proposed algorithm produced robust segmentation results by successfully mitigating the problems caused by low contrast, noise and bias field in the MR brain image. Dong and Peng [1] introduced a novel variation based approach for efficient segmentation of brain image by using simultaneous bias correction. To reduce the influence of noise and obtain a smooth segmentation, the nonlocal spatial regularization was used for the maintenance of fine structures in brain images. Huang et al [7] introduced a novel automatic tumor segmentation method to overcome the issues of high variations in the appearance of tumor and unclear tumor boundaries. The data distribution of different classes was considered in the Local Independent Projection-based Classification (LIPC) method by learning a soft-max regression model. Manikandan et al [2] presented a Real Coded Genetic Algorithm (RGA) with Simulated Binary Crossover based multilevel thresholding for the high-quality segmentation of T2 weighted MRI brain images. Due to the efficient global searching ability, the RGA with simulated binary crossover achieves higher entropy and lower standard deviation for all the images. Van Opbroek et al [8] used the transfer learning technique was used for the image segmentation process. The proposed transfer learning technique has achieved better segmentation performance than the common super vised learning approaches, while reducing the classification errors up to 60%. Ribbens et al [9] presented a data-driven probabilistic framework for the segmentation of heterogeneous set of brain MR images and image clustering. The segmentation accuracy was improved due to the combined segmentation and atlas construction. Caldairou et al [10] proposed an extended FCM based method for the unsupervised segmentation of the brain images. Occurrence of noise and intensity inhomogeneity in the image was handled efficiently by using the non-local (NL) framework. Wang et al [11] introduced a novel patch-driven level set method for the neonatal brain MR image segmentation by using sparse representation techniques. The accuracy of the proposed method for white and gray matter was increased. Ji et al [12] presented a modified possibilities FCM clustering algorithm for the fuzzy segmentation of MR images with intensity inhomogeneities and noise. The local contextual information was used to mitigate the noise and resolve the classification issues. Gao et al [13] introduced a novel algorithm for automatic lesion segmentation from multichannel MR images. Then, a nonlocal means technique was introduced to achieve spatially regularized segmentation, to overcome the influence of noise. Hancer et al [14] proposed a novel image segmentation method based on artificial bee colony algorithm (ABC) to extract brain tumors from MRI brain images. The proposed methodology was compared and analyzed on 9 MRI images obtained by using various techniques based on K-means, FCM and GA. Ji et al [15] proposed a Fuzzy Local Gaussian Mixture model (FLGMM) algorithm for the automated segmentation of brain MR image. The image segmentation accuracy of the

proposed algorithm was improved. Lu et al [16] presented an automatic segmentation, non-rigid registration and detection of tumor in the cervical MR data by using a unified Bayesian framework. Reddy et al [17] presented a novel brain tumor segmentation approach for effectively manipulating the texture information from multi-parametric MRI. The classifier was used to generate the confidence surface to obtain the likelihood of each pixel for the detection of tumor region. Koley and Majumder [18] introduced a Cohesion based Self-Merging algorithm for the segmentation of brain MRI image, to detect the exact location of brain tumor by using partitional K-means clustering algorithm. The computational complexity and computation time of the proposed approach were reduced and the exact location of tumor was obtained. Selvakumar et al [19] used a computer aided method for the segmentation and detection of brain tumor. Finally, approximate reasoning was used for evaluating the shape and position of tumor. Subbanna et al [20] presented an entirely automatic hierarchical probabilistic framework for the segmentation of brain tumors from the multispectral brain MRI image. Ji et al [21] proposed a generalized rough FCM (GRFCM) algorithm was proposed for brain MR image segmentation. The robustness of the proposed algorithm with respect to the noise and bias field was observed from the experimental results and more accurate and reliable segmentation was achieved. Rajendran and Dhanasekaran [22] combined fuzzy clustering with the deformable model for segmenting the tumor region on MRI images. Paul et al [23] proposed an automated scheme for the segmentation of brain MRI image, by using FCM algorithm. The presence of degenerative disease was identified by detecting the reduction in the gray matter in the brain image. The major drawback of the FCM algorithm was the high computational time required for convergence. So, the cluster center and membership value updating criterion were modified to improve the computational rate of the FCM algorithm. Shasidhar et al [24] used the modified FCM algorithm to detect the brain tumor. The segmentation efficiency and convergence rate of the modified FCM algorithm were improved. Mukhopadhyay and Maulik [25] introduced a novel multiobjective genetic fuzzy clustering scheme for the segmentation of multispectral MR image of human brain. Wang et al [26] proposed a novel patch-driven level set method for the segmentation of neonatal brain images with the help of the sparse representation techniques. Benaichouche et al [27] used an improved FCM clustering algorithm for the segmentation of brain image. The Mahalanobis distance was used to reduce the influence of the geometrical shape of the different classes. Then, the clustering errors were corrected and the misclassified pixels were reallocated for refining the segmentation results. The presence of noise will vary the pixel intensity. This affects the segmentation of the brain image and detection of the exact location of the tumor. Occurrence of inhomogeneous intensities in the brain MRI images may cause due to the bias field and heavy noise. Since, the existing image segmentation algorithms typically depend on the homogeneity of image intensities, it fail to provide accurate segmentation results. Hence, this paper proposes a novel TPC based segmentation technique for the effective segmentation of brain MR image and exact detection of the location of brain tumor.

III. NOVEL TPC BASED MRI BRAIN IMAGE SEGMENTATION TECHNIQUE

This section explains about the proposed TPC based MRI brain image segmentation technique. The pre-processing involves adaptive median filtering, image normalization and image enhancement. An adaptive median filter performs filtering of the brain MRI image, to remove the impulse noise such as salt and pepper noise from the image. Edge detection using Canny is used for detecting edge of skull from MRI brain image. The morphological operation is applied to eliminate the skull from the input MRI image. The EGLCM is applied for the extraction of testing features to form a feature vector. Classification of the normal and abnormal images is performed by using a PNN classifier. The affine transform combined with FRFT is applied to extract the texture of tumor intensity level from the given input image. If the input image is classified as an abnormal image, then segmentation is done by using TPC segmentation process. Then, the growing pattern of tumor is analyzed and represented as a binary image output. Figure 2 shows the overall flow diagram of the proposed TPC based brain MRI image segmentation technique. The proposed approach involves the following steps □ Pre-processing □ Enhanced GLCM based feature extraction□ PNN classification □ Affine -transform based image registration□ TPC based image segmentation A. Pre-processing The pre-processing operation is performed to remove the noise contained in the image and enhance the visual appearance of the image. The three stages of the pre-processing operation are:□ Adaptive Median Filtering□ Image normalization □ Image enhancement. 1) Adaptive Median Filtering The adaptive median filter [28] performs spatial processing technique to determine whether the pixels in the image are affected by the impulse noise such as salt and pepper noise.

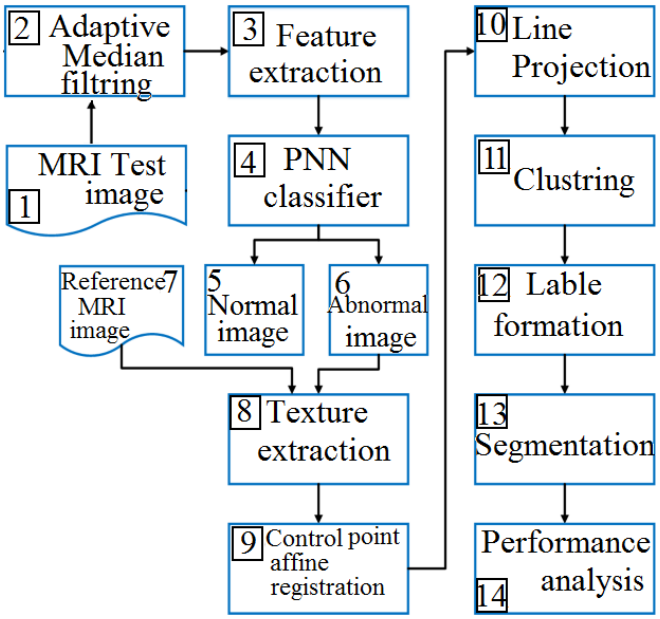

Figure 2 Overall flow diagram of the proposed TPC based brain MRI image segmentation technique

It compares each pixel with its surrounding neighbor pixels, to classify the pixels as noise. A pixel that differs from the majority of its neighboring pixel is considered as impulse noise. Then, the noise pixels are replaced with the median value of the

neighborhood pixels. The size of a window around each pixel varies corresponding to the median value of the pixels in the 3 × 3 window. The size of the window is increased, if the median value is detected as an impulse. Then, it is verified whether the center pixel of the window is an impulse or not. If it is detected as a noise, the new value of the center pixel in the filtered image is considered as the median value of the pixel in the window. The center pixel value in the filtered image remains unchanged, if the center pixel is detected as a non impulse. Unless the considered pixel is detected as an impulse, the gray-scale value of the pixel in the filtered image remains same as the gray-scale value of pixel in the input image. Thus, the filter provides dual advantage including the removal of impulse noise from the image and reduction of distortion in the image. The median values are updated iteratively using the new pixels, thus reducing the computational overhead.

Adaptive Median Filtering Algorithm

Input: MRI brain image *'I'* **Output:** Preprocessed Image, *'Y'*Step 1: Initialize window size (3×3).
Step 2: Extract Connected Components, CC.
Step 3: $I = I(dx) = \max(CC)$
Step 4: $I = I(dx)$//Update Image with maximum connected component of pixel.
Step 5: ***for*** (i = 2 to *Row_ Size*(I) −1) //'i' Row size of image
Step 6: ***for*** (j = 2 to *Column_ Size*(I) −1) //'j' *Column* size of image
Step 7: $temp=I_{i-1\ to\ i+1,\ j-1\ to\ j+1}$//Project window over image matrix as, temp
Step 8: ***if*** ((temp (5) ~ temp (Boundary)) > temp (5)) //Check neighboring Pixel variation
Step 9: *Y (i, j) = Avg. (temp);*
Step 10: ***else***
Step 11: *Y (i, j) = median (S)*;
Step 12: ***End if***
Step 13: ***End for 'j'***
Step 14: ***End for 'i'***

The pseudo code for the adaptive median filtering algorithm is given above. The pixel components are extracted and the image is updated with the maximum pixel components. The image matrix is generated and window is projected for the specific size of the rows and columns of the matrix. Then, the neighboring pixel variation is checked. If the boundary value is high, then the mean value of the pixels is obtained. Otherwise, the median value is obtained. The window is subsequently moved to the following location in the image, based on the neighboring pixel variation. If there is no variation, the median value is determined. Figure 3(a) and Figure 3 (b) show the input images and Figure 3(c) and (d) show the filtered images. Advantages • the adaptive median filter preserves detail and smoothens non-impulsive noise. • Reduces distortion such as excessive thinning or thickening of object boundaries.*2) Image Normalization* In our proposed work, the image normalization is applied for detecting and eliminating skull from original image input. In this image normalization, canny edge detection method is used for detecting edge of skull from MRI brain image.

a) Edge Detection using Canny

Edge detection is an image processing technique used to find the boundaries of objects within the image.

Edge detection is an image processing technique used to find the boundaries of objects within the image. Canny method [4] is the most powerful and optimal edge-detection method. Since the Canny method uses two different thresholds to detect the strong and weak edges, it is different from other edge detection methods.

It includes the weak edges in the output only if they are connected to the strong edges. The first step of canny edge detection method is to remove the noise in the image by using a Gaussian filter. Here, the Canny implements the 3×3 matrix as filter coefficient. This is given as:

-1	0	1
-2	0	2
-1	0	1

G_x

1	2	1
0	0	0
-1	-2	-1

G_y

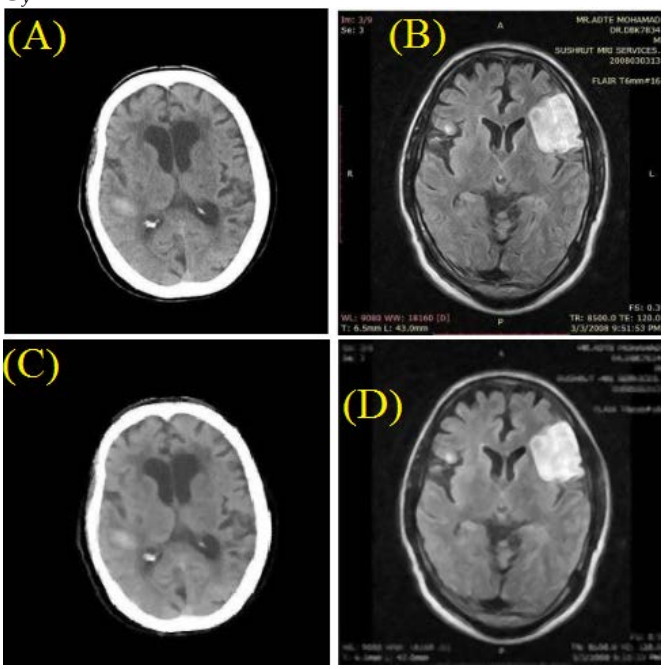

Figure 3(a) and (b) Input images and Figure 3(c) and (d) Filtered images

Then, the smoothened image is filtered with a Sobel kernel and vertical direction *G y* [4] in the horizontal direction *G x* to get first derivative in both the directions. From these two images, the edge gradient and direction for each pixel are computed. The magnitude at each gradient is estimated as,

$$|G| = |G_x| + |G_y| \quad (1),$$

$$G_x(x,y) = \frac{Y_{i,j+1} - Y_{i,j-1} + Y_{i-1,j+1} - Y_{i-1,j-1} + Y_{i+1,j+1} - Y_{i-1,j-1}}{2} \quad (2),$$

$$G_y(x,y) = \frac{Y_{i+1,j} - Y_{i-1,j} + Y_{i+1,j-1} - Y_{i-1,j-1} + Y_{i+1,j+1} - Y_{i-1,j+1}}{2} \quad (3)$$

Where, '*Y*' is the filtered image, '*i*' and '*j*' are the row and column limit of image pixel and '*Gx*' and '*G*' are the gradients at the '*x*' and '*y*' direction. $Angle(\theta) = \tan^{-1}\frac{G_x}{G_y}$ (4)

Usually, the gradient direction is always perpendicular to the edges. It is rounded to the vertical, horizontal and two diagonal directions. Figure 4(a) and Figure 4(b) show the output images of the edge detection process.

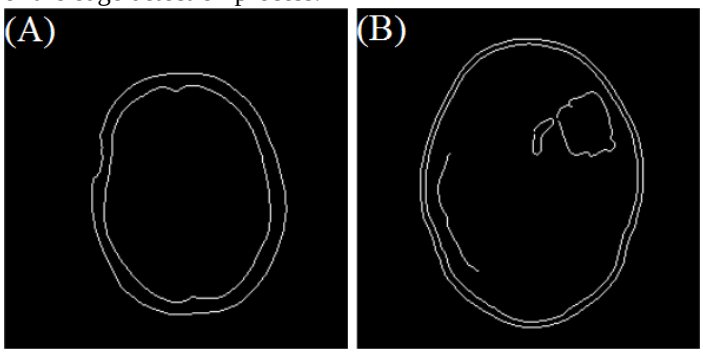

Figure 4(a) and (b) Output images of the Edge Detection process

From this edge information, the pixels in the edge image are considered as zero from the filtered image. Figure 5(a) and Figure 5(b) show the images with pixels of zero values at the edges.

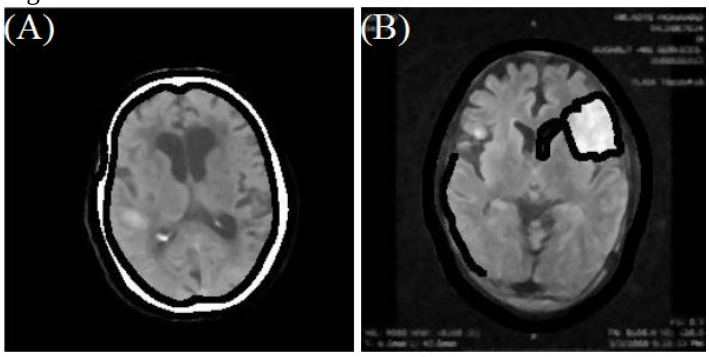

Figure 5(a) and (b) Images with pixels of zero values at the edges

After estimating the gradient magnitude and direction, the image is scanned completely to remove any unnecessary pixels that may not constitute the edge. For this, local maximum of every pixel in its neighborhood along the direction of gradient is checked. Then, the connected components are extracted to verify whether the unwanted pixels are present or not. The algorithm for connected component extraction is described below:

Algorithm for Connected Component extraction

Input: Filtered Image '*Y*' **Output:** Labeled Connected Components '*LB*' and Normalized image '*Y*'**Procedure**

Step 1: Convert Filtered image into Binary,'*B*'.
Step 2: initialize Label, *L=1;*
Step 3: ***for*** (i = 1 to *Row_Size* (*B*)) //'i' Row size of image
Step 4: ***for*** (j = 1 to *Column_Size* (*B*)) //'j' Column size of image
Step 5: $LB_{(ij)} = L$; // Allocate Label
Step 6: *Nt* = *Neighbors* (i, j) Collect Neighbor Pixel
Step 7: ***for*** (*t = 1 to length* (*N* (i, j))
Step 8: ***if*** (B (*N* (t))) ==-1
Step 9: LB (*N*(*t*)) = *L*; //Update Label
Step 10: ***end if***;
Step 11: end for'*t*'
Step 12: *L = L + 1;*
Step 13: end for '*j*'
Step 14: end for '*i*'
Step 15: *Y = Y* – max (*LB*).

The filtered image is converted into binary and label is initialized. Label is allocated to the pixels in the image. The neighbor pixel is collected. The labeled connected component is obtained based on the size of the neighboring pixel values. Figure 6(a) and Figure 6(b) show the images after removal of unnecessary pixels at the edges. The erosion and dilation operations are applied to eliminate the skull from the input MRI image. In the morphological operation, the value of each pixel in the output image is determined based on the comparison of the corresponding pixel in the input image with its neighboring pixels. Figure 7(a) and Figure 7(b) show the input MRI brain image after elimination of skull.

3) Image Enhancement

GMM based intensity equalization method is implemented to enhance the contrast of the MRI brain image. The GMM [29] is used for modeling the gray-level distribution of the image.

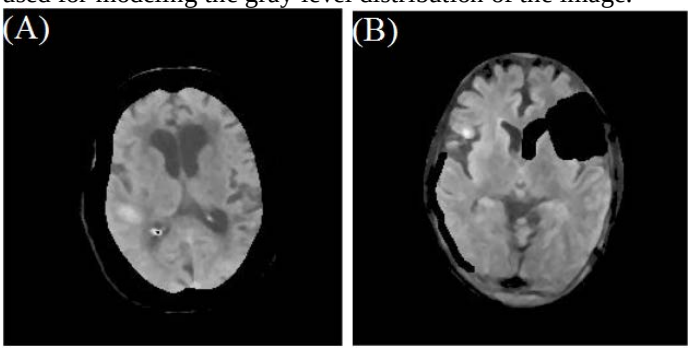

Figure 6(a) and (b) Images after removal of unnecessary pixels at the edges

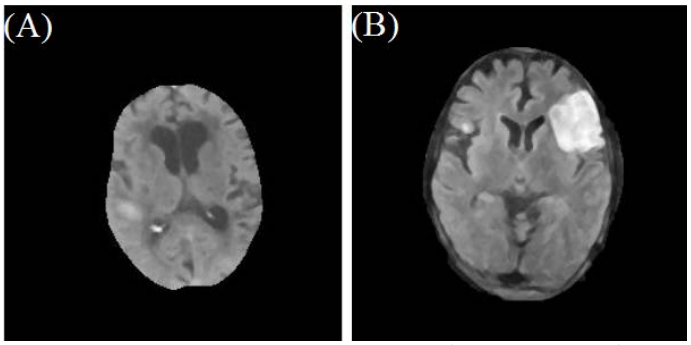

Figure 7(a) and (b) Input MRI brain image after elimination of skull

The dynamic range of the image is partitioned into input gray level Intervals by using the intersecting points of the Gaussian components. The gray levels of the pixels in each and every input interval are transformed into the appropriate output

graylevel interval to generate a contrast equalized image. This transformation process is performed according to the Cumulative Distribution Function (CDF) of the input gray-level interval and main Gaussian component. The lower weight is assigned to the Gaussian components with less variances than the Gaussian components with higher variances, to represent the homogeneous regions in the image histogram. The components are weighted by using the gray-level distribution, while mapping the input interval to the output interval. The Gaussian Kernel Function is defined as:

$$f_g(x) = \frac{1}{\sqrt{2\pi\sigma^2}} \exp\left[\frac{-(x-a)^2}{2\sigma^2}\right] (5)$$

The Gaussian mask (G_m) [30] is given as

$$G_m = \begin{bmatrix} (01)(04)(07)(04)(01) \\ (04)(16)(26)(16)(04) \\ (07)(26)(41)(26)(04) \\ (04)(16)(26)(16)(04) \\ (01)(04)(07)(04)(01) \end{bmatrix} \left(\frac{1}{273}\right) (6)$$

Image Enhancement Algorithm

Input: Normalized image, 'Y' Output: Enhanced image, '*Y*'
Step 1: Apply Gaussian Filter to the Normalized image '*Ye*'.
Step 2: Calculate Standard Deviation of '*Y*' by using equation (7)
Step 3: Calculate Mean value of '*Ygg*' by using equation (8)
Step 4: $L_1 = M - 10*S_1$;
Step 5: $L_2 = M - 10*S_2$;
Step 6: Update Y_g based on Limit *g* L_1 and L_2
Step 7: $Mw = Max\ (Y_g)$;
Step 8: Output the enhanced image obtained by using the equation (10)
The image enhancement algorithm is described above. The Gaussian filter is applied to the normalized image. The standard deviation of the normalized image is calculated by using:

$$S = \sqrt{\frac{1}{N}\sum_{i=1}^{N}(Y_{gi} - \mu)^2} \quad (7)$$

'μ' is the average value of the normalized image. Then, the mean value of the normalized image is computed using:

$$M = \frac{\sum Y_g}{N} (8)$$

The upper and lower limits are computed and the normalized image is updated based on the limits.

$$Y_g = \{Y_g, if\ (Y_g > L_1)\ \&\ (Y_g > L_2)\} (9)$$

Finally, the enhanced image is obtained based on the maximum intensity value for the normalized image.

$$Y_e = \frac{Y_g}{Mw} (10)$$

B. Feature extraction

Enhanced GLCM approach is applied for extracting texture based features from the image. The extracted features contain the relevant information of the image. It can be used as an input to the classifier for image classification and segmentation.

1) Enhanced GLCM

During the statistical texture analysis, the texture features are computed from the perceived combinations of the intensities of pixels at the specified positions in the image. The statistics are classified into first, second and higher-order statistics, according to the number of pixels in each combination. GLCM [31] is used to define the textural features and extract the second-order statistical texture features from the image. The values of the co-occurrence matrix elements present the relative frequencies with which two neighboring pixels are separated by a distance 'd'. The gray level of the pixels is denoted as '*i*' and '*j*'. The pixels are separated by the distance *(Δx, Δy)* within a given neighborhood. The number of rows and columns in the GLCM is equal to the number of gray levels in the image. The matrix element *P (i, j|d,ɵ)* contains the second order statistical probability values for the variation between the gray levels at a particular displacement distance '*d*' and at a particular angle '*ɵ*'. The GLCM features are described below:

a) Contrast

Contrast is defined as the measure of the local variations in the intensity between the neighboring pixels in the image. Contrast affects the view ability of details in an image. It is given by:

$$C_t = \sum_{a}^{N}\sum_{b}^{N}(a-b)^2\, p(a,b) (11)$$

Where 'C_t' is a contrast value, '*N*' denotes the number of various gray levels, '*p*' represents the probability value, and '*a*' and '*b*' represents the gray levels. The contrast value is found to be high, if there is large amount of variations present in the image. Its value is '0' for a constant image.

b) Correlation

Correlation is performed to extract information from the images. Correlation measures the joint probability occurrence of the specific pixel pairs. It is the linear dependency measure of gray levels on the neighboring pixels or specified points on the texture image. The correlation value is high for the similar gray-level regions. Correlation value is '+1' for a perfectly positively image and '-1' for negatively correlated image. It is given as $C_r = \sum_{a}^{N}\sum_{b}^{N}\frac{p(a,b) - \mu_x\mu_y}{\sigma_x\sigma_y} (12)$ Where μ_x, μ_y, and σ denotes the mean value, standard deviations of *p(a)* and *p(b)*, respectively. *C* represents a correlation value.

c) Cluster Prominence

Cluster prominence is also a measure of asymmetry. When the cluster prominence value is high, the image is less symmetric. If the prominence value is low, there is a peak in the GLCM matrix around the mean values. For an ultrasound image, a low cluster prominence value indicates small variation in gray-scale.

$$C_p = \sum_{a=0}^{N-1}\sum_{b=0}^{N-1}\{a+b-\mu_x\mu_y\}^4 * p(a,b) \quad (13)$$

d) Cluster Shade

Cluster shade is a measure of the skewness of the matrix and perceptual concepts of uniformity. When the cluster shade is high, then the image is asymmetric.

$$C_S = \sum_{a=0}^{N-1}\sum_{b=0}^{N-1}\{a+b-u_x-u_y\}^3 * p(a,b) \quad (14)$$

e) Dissimilarity

Dissimilarity is a measure of level of dissimilarity of two neighboring pixels. During the dissimilarity measure, there is a linear increase in the weight. In the Contrast measure, weights increase exponentially as one moves away from the diagonal.

$$D = \sum_{a,b=1}^{N} C_{a,b}|a-b| \quad (15$$

f) Energy

Energy is defined as a textural uniformity measure of the pair of pixels. The energy values are high, when the gray level distribution exhibits the constant or periodic form. It is defined as: $E = \sum_{a}^{N} P^2(a,b)$ (16)

g) Entrop

Entropy (H) is a measure of the uncertainty associated with a random variable. It is determined by:

$$Ent = \sum_{a=0}^{N}\sum_{b=0}^{N} p(a,b)\log p(a,b) \quad (17)$$

Therefore, the entropy value is lower for a homogeneous image and higher for the heterogeneous image.

h) Homogeneity

Homogeneity measures the uniformity of the non-zero entries in the matrix. The homogeneity is measured while assuming the larger values for smaller gray tone differences in the pair of pixel elements. The homogeneity value is high along the diagonal, due to similarity of the gray level values of a lot of pixels. Homogeneity decreases with the increase in the contrast value, while maintaining the energy at the constant level. The homogeneity is defined as

$$C_h = \sum_a \sum_b \frac{P_d[a,b]}{1+|a-b|} \quad (18)$$

i) Homogeneityp

Homogeneityp is defined as the closeness of the distribution of elements in the GLCM to the diagonal. Its value ranges from 0 to 1. Homogeneity value is '1' for a diagonal *GLCM*

$$Homop = \sum_a \sum_b \frac{1}{1-abs(a-b)} X_{ij} \quad (19)$$

The homogeneity value is lower for the large variation in the gray values. This increases the contrast value. The homogeneity value is high, if the image has little variation. If there is no variation in the image, then the homogeneity is equal to unity. Therefore, high homogeneity refers to the textures that contain ideal repetitive structures, while low homogeneity refers to the huge variation in the texture elements and their spatial arrangements. An inhomogeneous texture refers to an image with non-repetition of the texture elements and absence of spatial similarity.

j) Maximum probability

The probability value of the center pixel of the window exhibits the maximum value. Maximum probability values occur if a combination of pixels dominates the pairs of pixel in the window. $\max pro = |\max|_{a,b} P_d[a,b]$ (20)

k) Sum of squares: Variance

Variance is a measure of heterogeneity and variability of the gray level of the pixel pairs. High weights are applied to the elements that differ from the average value of *P(a,b)*. The variance value is high, when the gray-scale values of the pixels differ from the mean value. It is calculated as:

$$Var = \sum_{a=0}^{N-1}\sum_{b=0}^{N-1}(a-u_x)^2.p(a,b) + \sum_{a=0}^{N-1}\sum_{b=0}^{N-1}(b-u_x)^2.p(a,b) \quad (21)$$

l) Autocorrelation

The autocorrelation function of an image is used to assess the amount of regularity as well as the fineness/coarseness of the texture present in the image.

$$AC = \frac{XY}{(X-a)(Y-b)} \frac{\sum_{a=0}^{X-a}\sum_{b=0}^{Y-b} f(a,b)\,f(a+m,b+n)}{\sum_{a=1}^{N-1}\sum_{b=1}^{N-1} f^2(a,b)} \quad (22)$$

m) Average Kurtosi

Average Kurtosis (AK) measures the peak ness or flatness of a distribution of pixels relative to a normal distribution. The definition of kurtosis is given as

$$AK = \frac{\sum\left(\frac{1}{\sigma^4}\sum_a\sum_b((a*b)-\mu)^4(P_{ab})^{-2}\right)}{N} \quad (23)$$

'N' denotes the number of gray levels.

n) Average Skewness

Average Skewness (AS) describes the degree of asymmetry of the distribution of pixels in the specified window around its mean value. It represents the shape of the pixel distribution. The skewness is calculated using

$$AS = \frac{\sum\left(\frac{1}{\sigma^2}\sum_a\sum_b((a*b)-\mu)^2(P_{ab})\right)}{N} \quad (24)$$

C. PNN classification

PNN [32] is generally used in classification problems. When an input is applied, the pattern layer calculates the distance ranging from the input vector to the training input vectors. This produces a vector whose elements indicate the proximity of the input to the training input. The sum of the contribution for each class of inputs is calculated and total output is produced as a

vector of probabilities. Finally, the maximum value of these probabilities is chosen by the whole transfer function at the output obtained from the summation layer. Then, '1' is generated for the target class and '0' for non targeted class. The PNN architecture is shown in the Figure 8.

1) *Input layer*

Input layer consists of a single neuron for each predictor variable. The input neuron normalizes the range of the values of the predictor variables by subtracting the median value and dividing with the inter quartile range. The input neurons feed the values to each neuron in the pattern layer.

2) *Pattern layer*

Pattern layer comprises one neuron for each image in the training dataset. When presented with the vector of the input values obtained from the input layer, the pattern neuron calculates the Euclidean distance of the test data from the center point of the neuron and then applies the Radial Basis Function (RBF) kernel function using the summation of the input neuron values.

$$P_i = W_i * F_i \quad (25)$$

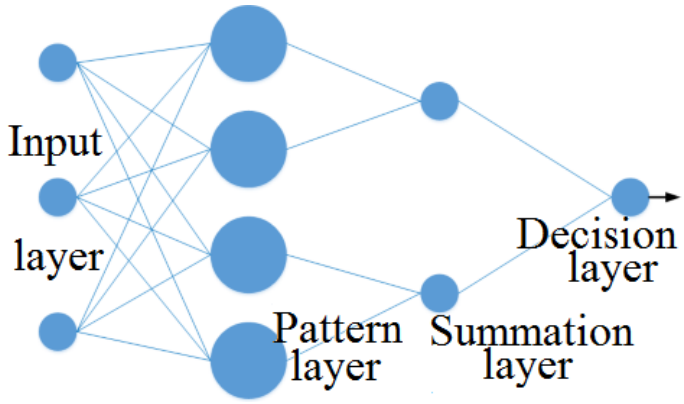

Figure 8 Architecture of PNN

Where W_i is the weight of the processing element and F_i is the input feature from the input layer. The pattern layer (i) classifies the input vectors based on highest matching with the input vector and generates an output. Therefore, a single classification category is generated for any input vector. If there is no relationship between the input patterns and the patterns of the pattern layer, then no output is generated.

3) *Summation layer*

The weighted value obtained from the pattern layer is fed only to the neuron in the summation layer that corresponds to the category of pattern neuron. The summation layer adds the values for the class. This is given as

$$C_j = \frac{\sum_{i=1}^{N_l} \exp\left(\frac{Pi-1}{\rho^2}\right)}{N_l} \quad (26)$$

Where 'N_l' is number of training set and 'ρ' is the smoothing factor.

4) *Decision layer*

The decision layer compares the weighted values for each target category collected in the summation layer and uses the highest vote to predict the target category. Finally, the PNN classifier performs classification of the input image as a normal or abnormal image.

D. Affine-transform based image registration

After detecting the abnormal category, then the image is passed to the image registration process. There are two images given as input to the image registration process. One is the given testing image and another one is reference MRI brain image. Here, the reference image for registration is extracted from tag from which the testing image was selected. Since for single person, there is more than 3 number of MRI images in the format of DICOM. These are tagged by proper labeling of each set of images. Either previous or next slice with respect to the tagging of the given image is selected. This selected image is pre-processed and image enhanced. In image registration, the affine transformation combined with FRFT is applied.

1) *Affine transformation*

Affine transformation is a linear mapping method that preserves points, straight lines, and planes. Sets of parallel lines remain parallel after the affine transformation. Generally, the affine transformation technique is used for correcting the geometric distortions or deformations that occur with non-ideal camera angles. It is one of the most commonly used methods for the registration of images. Image registration is the process of transforming different sets of data into a single coordinate system. It includes four simple transformations: translating, rotating, scaling and shearing. These operations preserve the co-linearity relationship between the points and the ratio of distances of points along a line. This means that the collinearity of the points before the transformation will remain same after the transformation. The main task of image registration process is to detect these affine transformations in order to build a coherent mapping between the source and target images. The transformation operations are controlled appropriately to construct a mathematical relationship between the two images. The transformation matrices are applied to each pixel location in the image to compute the desired transformation effect using matrix multiplication. An affine transformation corrects some global distortions in the images to be registered.

2) *FRFT*

The FRFT [33], [34] is a new transformation that performs the image analysis into the fractional time-frequency domain. FRFT simultaneously reflects the image information in the time domain and frequency domain, to enable unified time frequency transformation. If $f(x) \in L^2(R)^2$, its p-order FRFT is defined as

$$F_p(u) = \{F^p[f(x)]\}(u) = \int_{-\infty}^{\infty} K_p(u,x) f(x) dx \quad (27)$$ Where $K_p(u,x)$ is the FRFT kernel function.

$$K_p(u,x)=\begin{cases}\sqrt{\frac{1-j\cot\alpha}{2\pi}}\exp\left[\frac{x^2+u^2}{2\tan\alpha}-\frac{xu}{\sin\alpha}\right], \alpha\neq n\pi\\ \delta(x-u), \alpha=(2n\pi)\\ \delta(x+u), \alpha=(2n\pm1)\pi\end{cases}$$

(28)

Where $\alpha = p\pi/2$ represents the rotating angle. '*p*' denotes the order of the FRFT, $p \neq 2n$. $p \in [0,1]$ and $\alpha \in [0, \pi/2]$, $2\alpha\pi\in$. If *p=0*, then FRFT is *f(x)*. If *p=1*, FRFT is the conventional Fourier transform. The FRFT processed data includes both time and frequency domain information. When '*p*' ranges from 0 to 1, the FRFT result varies from the continuous transformation of the input function to the Fourier transformation. The angle of projection is calculated by using:

$$\theta_1 = \tan^{-1}(-y,x) = \frac{1}{2}i[\ln(1-i(-y,x)) - \ln(1+i(-y,x))]$$

(29)

$$R = \sqrt{x^2+y^2}$$ (30)

Where θ_1 is the angle of projection, *R* is the radius *x* and *y* are the coordinate points of image pixel.

$$Ang(\alpha) = \frac{(o-1)\pi}{N_l}$$ (31)

Where 'α' is the gradient angle, '*o*' is the interval limit and 'N_l' is the number of angles. The difference in the '*x*' and '*y*' coordinate points of the pixel is computed by using the equations:

$$ds = \sin(\theta)*\cos(\alpha) - \cos(\theta)\sin(\theta)*\cos(\alpha)$$ (32),

$$dc = \sin(\theta)*\cos(\alpha) + \cos(\theta)\sin(\theta)*\cos(\alpha)$$ (33)

The difference in the angle of projection is computed based on the difference in the coordinate points. $d(\theta) = \tan^{-1}(ds, dc)$ (34) The filter coefficient is calculated using the equation:

$$S_p = \exp\left(-[\frac{d\theta^2}{2\log(\sigma)^2}]\right)$$ (35)

$$f_0 = \frac{1}{\lambda}$$ (36)

$$f_0 = \frac{2rf}{C}$$ (37)

The Logarithmic Gabor Filter coefficient is calculated by using the relative frequency value. $S_p = \exp\left(-[\frac{\log\frac{R}{rf_0}}{2\log(\sigma)^2}]\right)$ (38)

The kernel function of the affine transform is computed by using the Logarithmic Gabor Filter coefficient and filter coefficient as follows:

$$K_p(u,x) = L_g * S_p$$ (39)

Where σ is the standard deviation of input image, *ds*, *dc* are the differences in '*x*' and '*y*', *d*θ is the difference in 'θ' and λ 'is the wavelength, '*C*' is the column length of image, *f* is the frequency, *rf* is the relative frequency, S_p is the filter coefficient, L_g and K_p is the Kernel Function of Affine transform. Figure 9(a) and (b) shows the textures of the image. Figure 10(a) and (b) show the testing images, (c) and (d) show the reference images and (e) and (f) show the registered images.

E. TPC based image segmentation

The TPC segmentation algorithm is applied to cluster out the background and tumor spot in the binary segmented output, if it is classified as an abnormal image. This segmentation process analyses the growing pattern of tumor and represents it as a binary image output. Pixel connectivity is a central concept of both edge-based and region-based approaches to the segmentation. The representation of the pixel connectivity defines the relationship between two or more pixels. To ensure the connection between two pixels, certain conditions on the brightness and spatial adjacency of the pixel are to be satisfied. In order to connect two pixels, the values of the pixels should be obtained from the similar set of values '*V*'. For a gray scale image, '*V*' denotes any range of gray levels for a binary image.

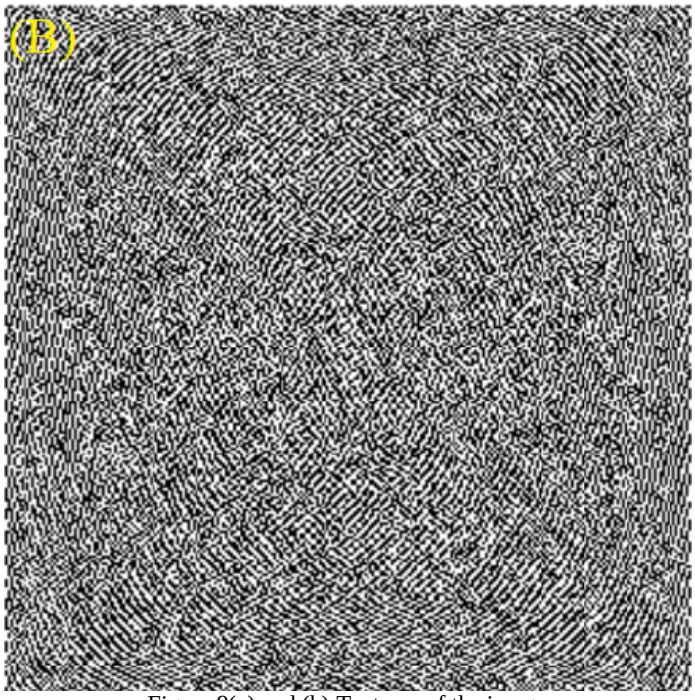

Figure 9(a) and (b) Textures of the image

The adjacency criterion for connectivity is formulated by introducing the neighborhood representation. For a pixel denoted as '*p*' with the '*x*' and '*y*' coordinate values, the set of pixels is given by:

$$R_{im} = \{(x+1, y), (x-1, y), (x, y+1), (x, y-1)\} \quad (40)$$

$$N_s(p) = R_{im}\{(x+1, y+1), (x-1, y-1), (x-1, y+1), (x-1, y-1)\} \quad (41)$$

Where '*x*' is the column coordinate value and '*y*' is the row coordinate values in the image. The value of the pixel '*p*' is obtained from a set of gray level intensity. The pseudo code for the image segmentation algorithm is explained below.

Image Segmentation Algorithm

Input: Fused image 'R_{im}' **Output:** Preprocessed Image, 'S_{im}'
Step 1: Initialize window size (3×3)
Step 2: Calculate Mean value of R_{im} using equation (47)
Step 3: *Mx* = max (R_{im})
Step 4: ***for*** (i = 2 to_ *Row size* (R_{im})-1) //'i' Row size of image
Step 5: ***for*** (j = 2 to Column_ *size* (R_{im})-1) *//'j' Column size* of image
Step 6: temp = $R_{im(i\text{-}1toi+1,\ j\text{-}1toi+1}$//Project window over image matrix as, temp
Step 7: ***if*** ((temp (5) ~ temp (Boundary)) > Min &&<Max) //Check neighboring Pixel variation.
Step 8: S_{out} *i j* =;
Step 9: ***else***
Step 10: S_{out} *i j* =0;
Step 11: *end if*
Step 12: *end for 'j*
'Step 13: *end for 'i*
'The mean value of the fused image is calculated by using the

$$M_n = \frac{\sum R_{im}}{N} \quad (42)$$

The window is projected for the specific size of the rows and columns of the image matrix. Then, the neighboring pixel variation is checked based on the maximum and minimum boundary values. If the neighboring pixel lies within the specific range, then the pre-processed image is generated. Figure 11 (a) shows the binary extracted initial cluster, Figure 11 (b) shows the labeled cluster and Figure 11 (c) shows the initial mask for segmentation. Figure 12 (a) and (b) shows the segmented images.

IV. PERFORMANCE ANALYSIS

The performance analysis results of the proposed TPC based brain MRI image segmentation technique is illustrated in this section. The performance of the PNN classifier for Eight Medulloblastoma Patients is evaluated by comparing it with the traditional Adaboost and enhanced Adaboost [35].

IV. PERFORMANCE ANALYSIS

The performance analysis results of the proposed TPC based brain MRI image segmentation technique is illustrated in this section. The performance of the PNN classifier for Eight Medulloblastoma Patients is evaluated by comparing it with the traditional Adaboost and enhanced Adaboost [35]. The metrics used for evaluating the performance of the proposed technique are

- ☐ Jaccard Coefficient
- ☐ Dice overlap
- ☐ True Positive Rate
- ☐ False Positive Rate

A real-time dataset is used for the performance analysis of the proposed work. In the real-time image, TR=8500, TE=120, WL=9080, WW=18160, FS=0.3, T=6.5 mm and L=43.0 mm. Oasis [36], Brainweb [37], MIDAS [38], Zenodo [39] and GE DICOM dataset [40] are used for performance evaluation. The Open Access Series of Imaging Studies (OASIS) [36] is a project developed for enabling free availability of the brain MRI datasets to the scientific community. OASIS is made available by the Alzheimer Disease Research Center at the King Abdulaziz University. It includes cross-sectional MRI data of 416 subjects aged from 18 to 96. 3 or 4 individual T1-weighted MRI scans are obtained for each subject. This also includes longitudinal MRI data of 150 subjects aged from 60 to 96. Each subject was scanned two or more times for 373 imaging sessions. Brainweb [37] is a Simulated Brain Database (SBD) that includes a set of realistic MRI data capacities produced by an MRI simulator. Currently, the SBD contains simulated brain MRI data based on two anatomical models: normal and multiple sclerosis (MS). For both anatomical models, full 3-dimensional data volumes have been simulated using three sequences (T1, T2, and proton-density (PD) weighted) based on the slice thicknesses, noise levels, and levels of intensity variation in the brain MRI images.

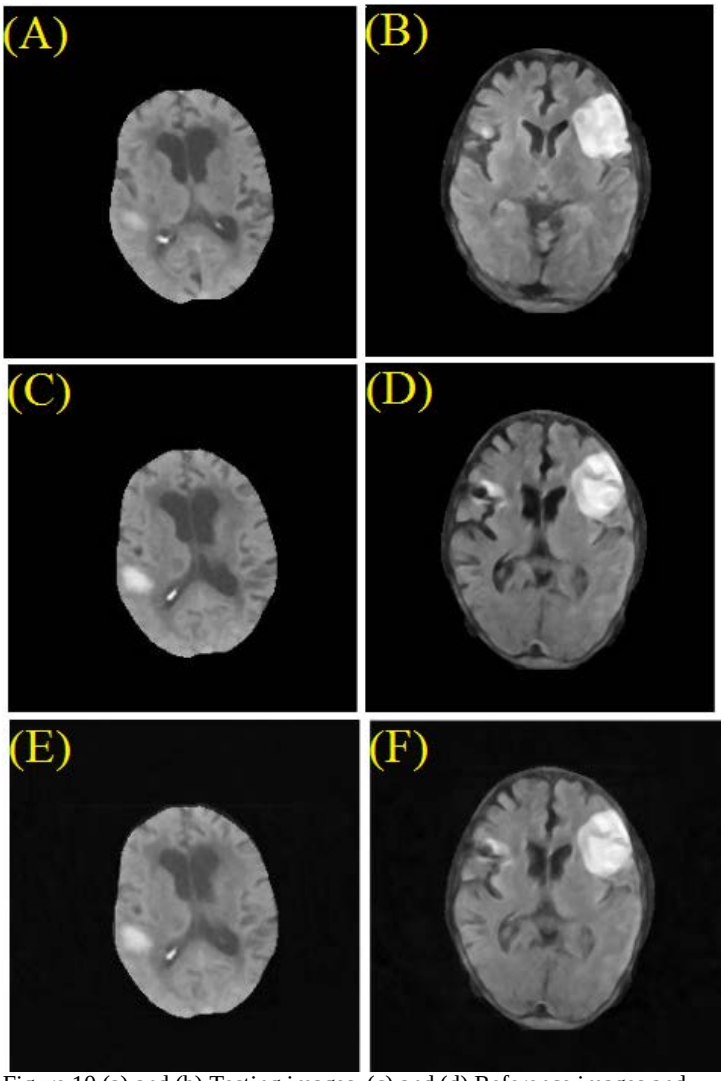

Figure 10 (a) and (b) Testing images, (c) and (d) Reference images and (e) and (f) Registered images

The brain images are obtained in three orthogonal views i.e., coronal, sagittal and transversal. In the simulated MRI volumes for Normal brain and Brain with Multiple Sclerosis Lesions, the parameter settings are fixed to 3 modalities, 5 slice thicknesses, 6 levels of noise, and 3 levels of intensity variation. MIDAS [38] is a MR database includes MRI images of the brain of 100 healthy subjects in which 20 patients were scanned per decade. Images include T1 and T2 acquired at 1x1x1 mm3, Magnetic Resonance Angiography (MRA) acquired at 0.5 x 0.5 x 0.8 mm3, and Diffusion Tensor Imaging (DTI) using 6 directions and a voxel size of 2x2x2 mm3. Zenodo [39] includes a DICOM dataset of MR images of a normal male subject aged 52. The MRI scan is done at the Radiology Department at the King Abdulaziz University Hospital.

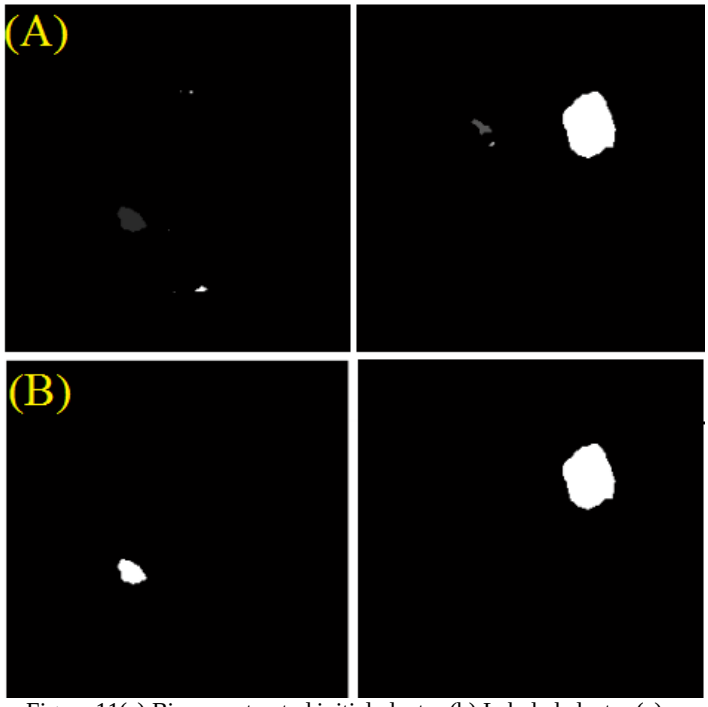

Figure 11(a) Binary extracted initial cluster (b) Labeled cluster (c) Initial Mask for segmentation

MRI cron is a brain imaging tool that uses NIfTI format for the analysis of the brain images. Two different scans are obtained for the same individual. The MRI cron shows the image orientation correctly, even if the scans are acquired at different orientations.

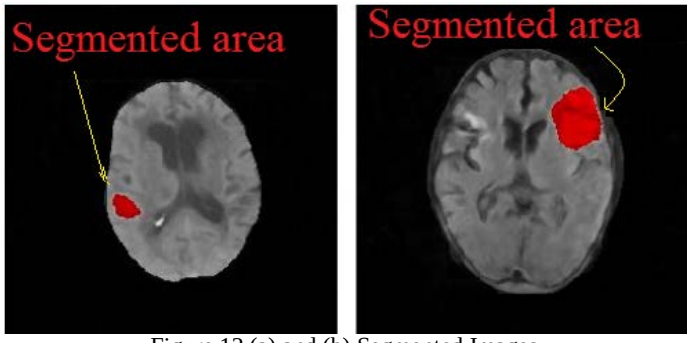

Figure 12 (a) and (b) Segmented Images

The T1-weighted longitudinal MRI brain images are used in our proposed work. The abnormality level of Brain tumor is benign, malignant and meta-static with Multi Sclerosis.

1. Oasis Database – 150 number of subjects and 373 number of images. Each subject contains minimum 2 number of Brain MRI image slices. Normal = 72 subjects. Abnormal = 78 subjects. 2. Brainweb image dataset – 362 numbers of images. Normal = 181 images. Abnormal = 181 images.3. MIDAS image dataset – 109 number of images. Normal = 109 images.4. Zenodo image dataset – 117 number of images. Normal = 117 images. 5. GE DICOM dataset – 148 number of Slices for each contains 5 number of images. Totally 740 number of brain MRI images Normal = 124 Slices. Abnormal = 124 Slices.Total number of images used: 1701Normal images: 1171 Abnormal Images: 530 1190 images are used for training and 510 images are used for testing

A. Jaccard coefficient

The Jaccard coefficient is another widely used spatial overlap measure of similarity indices for labeled regions.Generally, it is written as

$$Jaccard = \frac{(|TP|)}{(|TP| + |FP| + |FN|)} (43)$$

It is defined as ratio of the number of image samples with correct and incorrect prediction of tumor.

$$Jaccard = \frac{|A|}{(|A| + |B|)} (44)$$

Where 'A' is the number of brain image samples in which the presence of tumor is confirmed and 'B' is the number of samples in which the tumor detection decisions mismatch.*B.*

B. Dice overlap

The Dice overlap is a significant measure of the extent of spatial overlap between the two similarity labeled regions over the average volume of these regions. Furthermore, Dice is represented as the summation of a set of multiple labeled regions in the original image 'A' and reference image 'G'. It is given

as: $Dice = 2\frac{|A \cap G|}{(|A| + |G|)} (45)$ $Dice = 2\frac{|TP|}{(|TP| + |FP| + |FN|)} (46)$ $Dice = 2\frac{A}{A + B} (47)$

C. True Positive

*Rate*The True Positive Rate (TPR) is the ratio of the positive cases that are correctly classified as positive. TPR is defined as the proportion of the tumor pixels that are correctly classified as tumor by the classifier. $TRP = 2\frac{TP}{TP + FN} (48)$

D. False Positive

Rate The False Positive Rate (FPR) is the ratio of negatives cases that are incorrectly classified as positive. The FPR is defined as the proportion of the non-tumor pixels that are incorrectly classified as tumor by the classifier. This is calculated by using the equation:

$$TRP = 2\frac{FP}{FP + TN} (49)$$

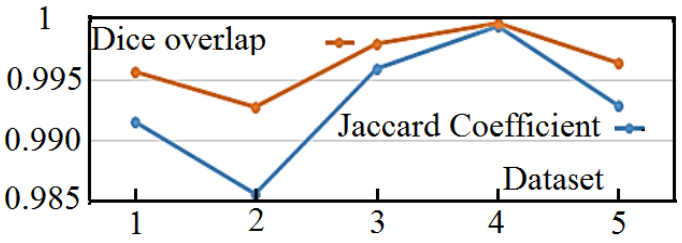

Figure 13 Comparative Analysis of Jaccard Coefficient and Dice overlap

Figure 13 shows the graph illustrating the comparative Analysis of the Jaccard Coefficient and Dice overlap of the proposed technique corresponding to five different datasets. The Jaccard Coefficient and Dice overlap of the proposed technique is higher for the fourth dataset, when compared to other datasets. This implies that the proposed approach achieves better performance in terms of Jaccard Coefficient and Dice overlap.

E. Confusion Matrix

A confusion matrix shows the number of the correct and incorrect classification results of the PNN classification method. Usually, the performance of the PNN classification method is evaluated by using the data in the matrix. This confusion matrix is defined as

Actual	Predicted	Positive	Negative
Positive		TP	FN
Negative		FP	TN

Where, 'TP' is the number of correct classification about the presence of tumor in the brain image, 'FN' is the number of incorrect classification of the presence of tumor region as the normal region, 'FP' is the number of incorrect classification of the normal region as the tumor region and 'TN' is the number of classification of the normal images. Figure 14 shows the confusion matrix for the proposed technique. This shows the classification rate of the normal image is higher. Hence the classification rate of the proposed technique is improved.

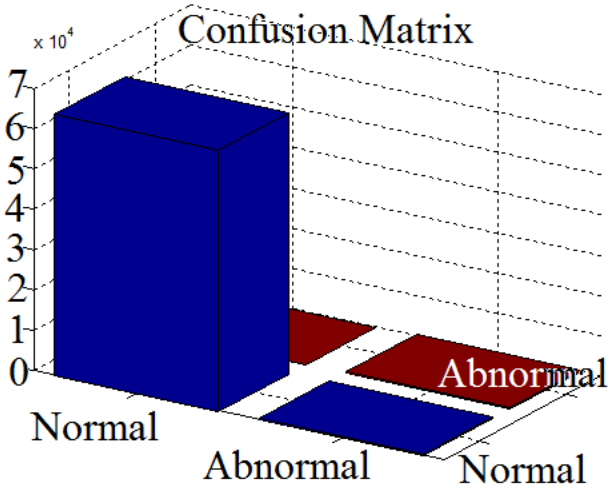

Figure 14 Confusion matrix

F. ROC graph

ROC graph indicates the comparative analysis between the True positive Rate and False Positive Rate of the proposed TPC based Image Segmentation Technique (IST) and existing approaches. ROC analysis is used in clinical applications to quantify the accuracy of the diagnosis systems in the detection of normal regions and tumor regions.

The proximity of the curve to the upper left-hand corner indicates the higher discrimination capability of the proposed technique. A feature set including intensity, PTPSA [35], multi-FD and text on [41] features is compared with the proposed

technique. Figure 15 shows the ROC graph for the proposed TPC based IST and (a) intensity and PTPSA, (b) intensity and multi-FD, (c) intensity, PTPSA and multi-FD, (d) intensity and texton, and (e) intensity, PTPSA, multi-FD, and texton feature combinations. From the figure, it is clearly evident that the proposed technique outperforms the existing feature combinations. Table I shows the comparative analysis of the performance of PNN Classifier for Eight Medulloblastoma Patients.

Table 1 Comparative analysis of the performance of PNN classifier for eight medulloblastoma patients.

PERFORMANCE OF PNN CLASSIFIER FOR EIGHT MEDULLOBLASTOMA PATIENTS				
Classification Method	**TPR**	**FPR**	**Jaccard**	**Dice**
Traditional Adaboost	0.79	0.36	0.58	0.73
Enhanced Adaboost	0.81	0.39	0.58	0.73
PNN Classifier	0.985	0.0085	0.993	0.9965

The TPR, FPR, Jaccard and Dice of the traditional Adaboost, enhanced Adaboost and PNN classifier are compared. The table shows that the PNN classifier achieves high TPR, Jaccard and Dice and low FPR, when compared to the traditional Adaboost and enhanced Adaboost. The PNN classifier achieves 98.5% TPR and very low FPR. Jaccard of the PNN classifier is 99.3% and Dice value is 99.65%.

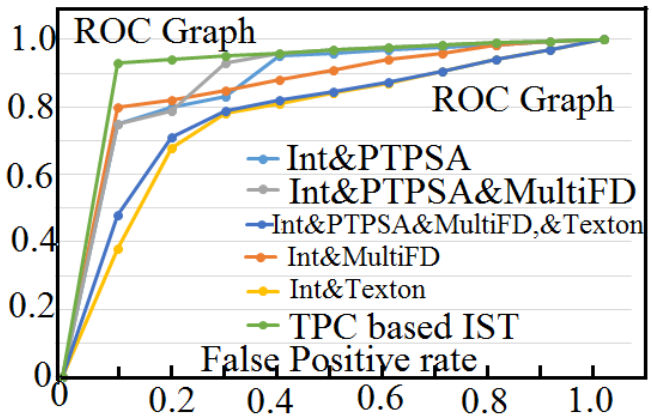

Figure 15 ROC graph for the proposed technique and feature combinations

G. Accuracy, Sensitivity and Specificity

Accuracy is defined as the measure of correctly classification results of the tumor region. Accuracy varies corresponding to the sensitivity. Sensitivity and specificity are the two significant statistical measures of the performance of binary classification test in the medical applications. Sensitivity is a true positive measure indicating the correct classification rate of the tumor region in the image. Specificity is a measure of true negative classifications that denotes the incorrect classification of the tumor region in the image.

$$Accuracy = \frac{N_{TP} + N_{TN}}{N_{TP} + N_{TN} + N_{FP} + N_{FN}} (50)$$

$$Sensitivity = \frac{N_{TP}}{N_{TP} + N_{FN}} (51)$$

$$\text{Specificity} = \frac{N_{TP}}{N_{TP} + N_{FN}} (52)$$

Where N_{TP} is the true positive measurement, *N TN* is the true negative measurement, *N FP* is the false positive measurement (portion of the image incorrectly classified as tumor), and *N FN* is the false negative measurement (portion of the image incorrectly classified as not a tumor)

H. PPV and NPV

The PPV and NPV are the two metrics that are useful in the clinical applications, during the availability of the test results. The PPV is the probability of positive detection of tumor and the NPV is the probability of the negative tumor detection results. These two measures are highly influenced by the prioprevalence of tumor. PPV increases with a higher prevalence tumor while the NPV decreases with a higher prevalence.

$$PPV = \frac{TP}{TP + FP} (53)$$

$$PPV = \frac{Sensitivityxprevalence}{(Sensitivityxprevalence) + (1 - Spicivity)(1 - prevalence)}$$

(54)

$$NPV = \frac{TN}{TN + FN} (55)$$

$$NPV = \frac{Spicivity(1 - prevalence)}{(Spicivity)x(1 - prevalence) + (1 - Spicivity)(1 - prevalence)}$$

(56)

I. Positive and negative Likelihood

Likelihood ratio provides a numerical measure of the effect of the result on probability. It is an alternate method of evaluating the performance of the tumor diagnosis. Because the tumor detection results can be positive or negative, there are two likelihood ratios for each test. The positive likelihood ratio (*LRP*) represents the amount of increase in the detection probability, if the tumor detection result is positive. The negative likelihood ratio (*LRN*) represents the amount of decrease in the detection probability, if the tumor detection result is negative. Positive Likelihood Ratio (LRP) is the ratio of the true positive tumor detection rate to the false positive rate.

$$LR_P = \frac{TP}{FP} (57)$$

$$LR_P = \frac{Sensitivity}{(1 - Spicivity)} (58)$$

Negative Likelihood Ratio (LRN) is the ratio of the false negative tumor detection rate to the true negative detection rate.

$$LR_N = \frac{TN}{FN} \quad (59)$$

$$LR_P = \frac{1 - Sensitivity}{Spicivity} \quad (60)$$

Correct Rate is defined as the correct detection rate of the presence of tumor in the MRI brain image. Error Rate is defined as the negative detection rate of the tumor**.**

Table II shows the values of performance metrics for the proposed technique. The inconclusive rate of the proposed technique is zero. The prevalence rate of the proposed technique is 0.9878. Hence, it is concluded that the proposed approach achieves high correct rate, last correct rate, classified rate, sensitivity, specificity, prevalence, accuracy, PPV, positive likelihood and low error rate, inconclusive rate, NPV and negative likelihood.

Table II Values of Performance Metrics for the proposed Technique

Performance Metrics Values	Values
Correct Rate	0.9931
Error Rate	0.0069
Last Correct Rate	0.9931
Last Error Rate	0.0069
Inconclusive Rate	0
Classified Rate	1
Sensitivity	1
Specificity	0.4584
Positive Predictive value	0.993
Negative Predictive Value	NaN
Positive Likelihood	4.0225
Negative Likelihood	NaN
Prevalence	0.9878
Accuracy	99.31%

V. CONCLUSION

The conclusion and future implementation of the proposed work are discussed in this section. The performance of various image segmentation techniques used for the analysis of human brain is affected by the artifacts such as random noise, intensity inhomogeneity, etc. To overcome the limitations of the existing image segmentation techniques, a novel TPC based segmentation technique is presented for the efficient segmentation of brain MRI image. The proposed approach enables detection of exact location of tumor in the brain. The PNN classifier is used to classify the images as normal or abnormal images. If the image is classified as abnormal, then TPC segmentation process is applied for clustering out the background and tumor spot in the binary segmented output. Finally, the performance of the PNN classifier is evaluated by comparing it with traditional Adaboost and enhanced Adaboost. The proposed technique achieves superior performance in terms of sensitivity, specificity, accuracy, error rate, correct rate, inconclusive rate, PPV, NPV, classified rate, prevalence, positive likelihood and negative likelihood. In future, this type of image segmentation technique is applied for both T1 and T2weighted Brain MRI images.

Conflict of Interest: The authors declare that they have no conflict of interest.

Compliance with Ethical Standards: Ethical approval: This article does not contain any studies with human participants or animals performed by any of the authors.

REFERENCES

[1] F. Dong and J. Peng, "Brain MR image segmentation based on local Gaussian mixture model and nonlocal spatial regularization," *Journal of Visual Communication and Image Representation*, vol. 25, pp. 827-839, 2014.
[2] S. Manikandan, K. Ramar, M. W. Iruthayarajan, and K. Srinivasagan, "Multilevel thresholding for segmentation of medical brain images using real coded genetic algorithm," *Measurement*, vol. 47, pp. 558568, 2014.
[3] G. E. Sujji, Y. Lakshmi, and G. W. Jiji, "MRI brain image segmentation based on thresholding," *International Journal of Advanced Computer Research*, vol. 3, pp. 97-101, 2013.
[4] A. S. Kulkarni and R. Kamathe, "MRI Brain Image Segmentation by Edge Detection and Region Selection."
[5] Y. Kong, Y. Deng, and Q. Dai, "Discriminative clustering and feature selection for brain MRI segmentation," *IEEE Signal Processing Letters*, vol. 22, pp. 573-577, 2015, 16
[6] Z. Ji, Y. Xia, Q. Sun, Q. Chen, and D. Feng, "Adaptive scale fuzzy local Gaussian mixture model for brain MR image segmentation," *Neurocomputing*, vol. 134, pp. 60-69, 2014.
[7] M. Huang, W. Yang, Y. Wu, J. Jiang, W. Chen, and Q. Feng, "Brain tumor segmentation based on local independent projection-based classification," *IEEE Transactions on Biomedical Engineering*, vol. 61, pp. 2633-2645, 2014.
[8] A. van Opbroek, M. A. Ikram, M. W. Vernooij, and M. de Bruijne, "Transfer learning improves supervised image segmentation across imaging protocols," 2015.
[9] A. Ribbens, J. Hermans, F. Maes, D. Vandermeulen, and P. Suetens, "Unsupervised segmentation, clustering, and groupwise registration of heterogeneous populations of brain MR images,"
IEEE Transactions on Medical Imaging, vol. 33, pp. 201-224, 2014.
[10] B. Caldairou, N. Passat, P. A. Habas, C. Studholme, and F. Rousseau, "A non-local fuzzy segmentation method: Application to brain MRI," *Pattern Recognition*, vol. 44, pp. 1916-1927, 2011.
[11] L. Wang, F. Shi, G. Li, Y. Gao, W. Lin, J. H. Gilmore, *et al.*, "Segmentation of neonatal brain MR images using patch-driven level sets," *NeuroImage*, vol. 84, pp. 141-158, 2014.
[12] Z.-X. Ji, Q.-S. Sun, and D.-S. Xia, "A modified possibilistic fuzzy c-means clustering algorithm for bias field estimation and segmentation of brain MR image,"

Computerized Medical Imaging and Graphics, vol. 35, pp. 383-397, 2011.
[13] J. Gao, C. Li, C. Feng, M. Xie, Y. Yin, and C. Davatzikos, "Non-locally regularized segmentation of multiple sclerosis lesion from multi-channel MRI data," *Magnetic resonance imaging*, vol. 32, pp. 10581066, 2014.
[14] E. Hancer, C. Ozturk, and D. Karaboga, "Extraction of brain tumors from MRI images with artificial bee colony based segmentation methodology," in *8th International Conference on Electrical and*
Electronics Engineering (ELECO), , 2013, pp. 516520.
[15] Z. Ji, Y. Xia, Q. Sun, Q. Chen, D. Xia, and D. D. Feng, "Fuzzy local Gaussian mixture model for brain MR image segmentation," *IEEE Transactions on Information Technology in Biomedicine*, vol. 16, pp.339-347, 2012.
[16] C. Lu, S. Chelikani, D. Jaffray, M. F. Milosevic, L. H. Staib, and J. S. Duncan, "Simultaneous nonrigid registration, segmentation, and tumor detection in MRI guided cervical cancer radiation therapy," *IEEE Transactions on Medical Imaging*, vol. 31, pp. 12131227, 2012.
[17] K. K. Reddy, B. Solmaz, P. Yan, N. G. Avgeropoulos, D. J. Rippe, and M. Shah, "Confidence guided enhancing brain tumor segmentation in multi parametric MRI," in *9th IEEE International Symposium on Biomedical Imaging (ISBI)*, 2012, pp. 366-369.
[18] S. Koley and A. Majumder, "Brain MRI segmentation for tumor detection using cohesion based self merging algorithm," in *IEEE 3rd International Conference on Communication Software and Networks (ICCSN)*, 2011, pp. 781-785.
[19] J. Selvakumar, A. Lakshmi, and T. Arivoli, "Brain tumor segmentation and its area calculation in brain MR images using K-mean clustering and Fuzzy Cmean algorithm," in *International Conference on Advances in Engineering, Science and Management (ICAESM)*, , 2012, pp. 186-190.
[20] N. K. Subbanna, D. Precup, D. L. Collins, and T. Arbel, "Hierarchical probabilistic Gabor and MRF segmentation of brain tumours in MRI volumes," in *Medical Image Computing and Computer-Assisted Intervention–MICCAI 2013*, ed: Springer, 2013, pp. 751-758.
[21] Z. Ji, Q. Sun, Y. Xia, Q. Chen, D. Xia, and D. Feng, "Generalized rough fuzzy c-means algorithm for brain MR image segmentation," *Computer methods and programs in biomedicine*, vol. 108, pp. 644-655, 2012.
[22] A. Rajendran and R. Dhanasekaran, "Fuzzy clustering and deformable model for tumor segmentation on MRI brain image: a combined approach," *Procedia Engineering*, vol. 30, pp. 327-333, 2012.
[23] G. Paul, T. Varghese, K. Purushothaman, and N. A. Singh, "A Fuzzy C Mean Clustering Algorithm for Automated Segmentation of Brain MRI," in *Proceedings of the International Conference on Frontiers of Intelligent Computing: Theory and Applications (FICTA) 2013*, 2014, pp. 59-65.
[24] M. Shasidhar, V. S. Raja, and B. V. Kumar, "MRI brain image segmentation using modified fuzzy cmeans clustering algorithm," in *International Conference on Communication Systems and Network Technologies (CSNT)* 2011, pp. 473-478.
[25] A. Mukhopadhyay and U. Maulik, "A multi objective approach to MR brain image segmentation," *Applied Soft Computing*, vol. 11, pp. 872-880, 2011.
[26] L. Wang, F. Shi, G. Li, W. Lin, J. H. Gilmore, and D. Shen, "Patch-driven neonatal brain MRI segmentation with sparse representation and level sets," in *IEEE 10th International Symposium on Biomedical Imaging (ISBI)*, 2013, pp. 1090-1093.
[27] A. Benaichouche, H. Oulhadj, and P. Siarry, "Improved spatial fuzzy c-means clustering for image segmentation using PSO initialization, Mahalanobis distance and post-segmentation correction," *Digital Signal Processing*, vol. 23, pp. 1390-1400, 2013.
[28] S. Shrestha, "Image Denoising using New Adaptive Based Median Filters," *arXiv preprint arXiv:1410.2175*, 2014.
[29] N. Girish and P. Smitha, "Survey On Image Equalization Using Gaussian Mixture Modeling With Contrast As An Enhancement Feature," in *International Journal of Engineering Research and Technology*, 2013. 17
[30] *Gaussian Smoothing*. Available: http://homepages.inf.ed.ac.uk/rbf/HIPR2/gsmooth.htm
[31] P. Mohanaiah, P. Sathyanarayana, and L. GuruKumar, "Image texture feature extraction using GLCM approach," *International Journal of Scientific and Research Publications*, vol. 3, p. 1, 2013.
[32] D. KETKAR, "CLASSIFICATION OF BRAIN TUMORS USING PRINCIPAL COMPONENT ANALYSIS AND PNN CLASSIFIER" *Proceedings of 12th IRF International Conference*, 17.05.2015, 2015.
[33] H. Tian, P.-g. Wang, and W. Zheng, "A new image fusion algorithm based on fractional wavelet transform," in *2nd International Conference on Computer Science and Network Technology (ICCSNT)*, 2012, pp. 2175-2178.
[34] P. Wang, H. Tian, and W. Zheng, "A novel image fusion method based on FRFT-NSCT," *Mathematical Problems in Engineering*, vol. 2013, 2013.
[35] A. Islam, S. Reza, and K. M. Iftekharuddin, "Multifractal texture estimation for detection and segmentation of brain tumors,"*Biomedical Engineering, IEEE Transactions on*, vol. 60, pp. 32043215,2013.
[36] OASIS. (30.01.2016). Available: http://www.oasisbrains.org/
[37] (30.01.2016). *Brainweb: Simulated Brain Database*. Available: http://brainweb.bic.mni.mcgill.ca/brainweb/
[38] E. S. Bullitt, J Keith; Lin, Weili. (30.01.2016). *MIDAS*. Available: http://insightjournal.org/midas/community/view/21
[39] W. R. B. Lionheart. (30.01.2016). *An MRI DICOM data set of the head of a normal male human aged 52*. Available:http://zenodo.org/record/16956#.VqxWD0C4Ey5
[40] (30.01.2016). *GE DICOM Dataset*. Available: http://www.mccauslandcenter.sc.edu/mricro/mricron/dcm2nii.html
[41] T. R. Raviv, K. Leemput, and B. H. Menze, "Multimodal brain tumor segmentation via latent atlases," *Proc. MICCAI-BRATS*, pp. 64-73, 2012.